Calculation of mixing times in single-phase and two-phase gas–liquid stirred tanks using positron emission particle tracking

W.J. Peace, D. Khoshdel, L. Gamet, F. Augier, C.R.K. Windows-Yule, M.J.H. Simmons

Chemical Engineering Science 330 (2026) 123846

Contents lists available at ScienceDirect

Chemical Engineering Science

journal homepage: www.elsevier.com/locate/ces

Calculation of mixing times in single-phase and two-phase gas–liquid stirred tanks using positron emission particle tracking

W.J. Peace [a], D. Khoshdel [a], L. Gamet [b], F. Augier [b], C.R.K. Windows-Yule [a], M.J.H. Simmons [a,*]

[a] School of Chemical Engineering, University of Birmingham, Edgbaston, Birmingham B15 2TT, United Kingdom
[b] IFP Energies Nouvelles, Rond-point de l'échangeur de Solaize, BP 3, Solaize 69360, France

ARTICLE INFO

Keywords:
Positron emission particle tracking
Mixing time
Lagrangian statistics
Stirred tanks

ABSTRACT

Positron Emission Particle Tracking (PEPT) enables novel insight into the mixing times of gas–liquid systems, particularly at high gassing rates, as it can interrogate opaque systems. Mixing times were obtained via analysis of Lagrangian statistics from PEPT, for single- and two-phase gas–liquid mixing experiments made in a $T = 0.2$ m diameter stirred tank equipped with either a radial pumping impeller (Rushton turbine, $D = T/3$) or axial pumping impeller (pitched blade turbine, $D = 0.4T$). Both Newtonian and non-Newtonian working fluids were employed using aqueous solutions of glycerol and carboxymethylcellulose, respectively, over a range of Reynolds numbers from 280 to 2300, in the high transitional to low turbulent flow regimes. These conditions were chosen to replicate the industrial processing of viscous media such as filamentous fungi. The approach was validated under single phase Newtonian conditions via benchmark acid-base decolourisation measurements and established empirical correlations, showing excellent agreement within ± 10%. Measurements made for gas–liquid Newtonian systems showed good agreement with established correlations in the dispersed aeration regime with both types of impellers. In non-Newtonian systems with gas void fractions of up to 9%, significant deviations in the measured mixing times from established correlations were observed, with values being up to 3–4 times greater in high viscosity, non-Newtonian media.

1. Introduction

Mixing in stirred tanks is ubiquitous for a wide range of industrial sectors including bulk and fine chemicals, pharmaceuticals, home and personal care, water and biochemicals. Control of mixing is necessary to ensure that the degree of homogeneity of each component within the media enables e.g. optimal conversion of reactants, generation of microstructure or minimisation of chemical gradients for optimal conditions for microbial growth and yield in bioreactions (Kukukova et al., 2009; Kukukova et al., 2008). A key bulk parameter used to evaluate mixing performance is the mixing time (also referred to in literature as the blend time), which is defined as the time required for a system to achieve a specified degree of homogeneity (Paul et al., 2004).

The use of mixing time as a parameter to characterise the performance of a stirred vessel has evolved from the earliest studies made of single-phase flows in stirred tanks. Although the reduction of mixing efficiency down to a single parameter such as a mixing time is a somewhat crude approach (Nienow, 1997), it is nevertheless a useful benchmark for industrial practitioners for process scale-up from bench scale to industrial sized equipment (Roussinova and Kresta, 2008; Gabelle et al., 2011; Magelli et al., 2013; Losoi et al., 2024). The seminal paper by Nienow (Nienow, 1997) in 1997 examined hydrodynamic theory, together with experimentally determined circulation times and mixing times and hydrodynamic measurements of agitator volumetric flow rate, to test the validity of an overall equation relating mixing time to scale-up parameters presented by various authors (Grenville, 1992; Ruszkowski, 1994). Circulation times can subsequently be estimated by dividing the fluid volume by the agitator flow rate if the appropriate integration limits are chosen to determine both the agitator flow rate and entrained flow in the circulation loops (Aubin et al., 2001). The overall equation for determining the time taken to obtain 95% homogeneity is well-established in the literature and of the form shown in Eq. (1), where the constant, A, correlated via numerous datasets (Grenville, 1992; Ruszkowski, 1994), has a value of 5.3 (Nienow, 1997).

* Corresponding author.
E-mail address: m.j.simmons@bham.ac.uk (M.J.H. Simmons).

https://doi.org/10.1016/j.ces.2026.123846
Received 28 October 2025; Received in revised form 25 February 2026; Accepted 21 March 2026
Available online 23 March 2026

$$\theta_{95} = A\frac{1}{N}\frac{1}{N_p{}^{1/3}}\left(\frac{D}{T}\right)^{-2} \quad (1)$$

Extension of these approaches to gas–liquid systems, which are highly relevant to industry e.g., for oxidation and reduction reactions and for fermentations, has led to a limited number of empirical correlations generated for specific geometries, such as those with high aspect ratios ($H/T \gg 1$) and using multiple impellers (Cooke, 1988; Vasconcelos et al., 1995; Zhao et al., 2001; Shewale and Pandit, 2006). Examples of some mixing time correlations published in literature are shown in Table 1.

1.1. Determination of mixing times from experiments and simulations

Measurement of mixing times is challenging given the complexities of the hydrodynamic conditions present in stirred tanks. Numerous studies exist using either pointwise measurements e.g. via addition of tracer and probes to measure conductivity (Grenville, 1992; Zhao et al., 2001; Zhang et al., 2009) or pH (Poulsen and Iversen, 1997; Zhang et al., 2014), or non-invasive optically-based whole field methodologies such as tracking of a fluorescent tracer or dye (Gabelle et al., 2011; Ramsay et al., 2016) decolourisation via chemical reaction (Cabaret et al., 2007; Rosseburg et al., 2018; Fitschen et al., 2021; Delbridge et al., 2023), or a change in temperature (Lee and Yianneskis, 1997). Probe-based measurements can lead to unrepresentative measurements of the mixing time, especially in non-Newtonian media when caverns and pseudo-caverns can be formed (Amanullah et al., 1998; Adams and Barigou, 2007; Simmons et al., 2009), if probe placement, and the injection point of the tracer media, is not carefully considered (Zhang et al., 2009; Fitschen et al., 2021). Additionally, their invasive nature may cause a change in the hydrodynamic conditions (Charalambidou et al., 2024) and thus the mixing characteristics. However, despite these caveats, probe measurements can be usefully applied to investigate opaque systems (Nere et al., 2003; Ascanio, 2015).

Although non-invasive optical based methodologies overcome some of the above limitations of use of probes, and provide whole field measurements of the overall system, their reliance on optical properties limits their use to transparent systems. Thus, they are not suitable for systems that are highly aerated, limiting gas volume fractions to low values (Aubin et al., 2004; Chung et al., 2009) or when the fluid itself is translucent or opaque. Alternative techniques such as Electrical Resistance or Impedance Tomography, have being successfully applied to determining local and global mixing times in two-phase gas–liquid stirred tank reactors of various configurations (Montante and Paglianti, 2015; Zak et al., 2022). However, this method is subject to resolution limitations of typically 5–10% of the tank cross section which limits its applicability to the study of the overall macromixing performance, and it does not work if the liquid and gas phases have similar electrical properties.

These limitations are particularly restrictive in industrial-relevant scenarios where optical access is not possible, such as with stainless steel vessels, opaque or complex media, or processes involving high levels of aeration. The analysis developed in this work uses Lagrangian trajectory information, obtained via non-invasive measurements, which overcomes these constraints.

Techniques for estimating mixing times from Computational Fluid Dynamics (CFD) simulations typically involve mimicking experimental methods, such as a decolourisation process (Cabaret et al., 2007). Examples have included the insertion of a passive scalar, which is fundamentally analogous to the injection of a dye (Coroneo et al., 2011). However, use of passive scalars introduces challenges which have been well documented in literature, highlighting that numerical diffusion of the passive scalar, an artefact of discretising the convection–diffusion equation on a finite grid, can often cause a significant underestimation of the mixing times. Efforts to compensate for this issue have included adjusting the turbulent Schmidt (*Sc*) number (Cappello et al., 2021), but this requires ad hoc adjustments of the parameter to match experimental data. Furthermore, the true value of the Schmidt number is not universal across a given stirred tank system and may vary with local flow conditions. Alternatively, CFD simulations with advanced methods such as Large Eddy Simulation (LES) with significantly fine grids can notably reduce the numerical diffusion (Hartmann et al., 2006; Yoon et al., 2015). However, these simulations are computationally expensive and may not be feasible for industrial-scale problems.

The application of discrete particle tracking in CFD simulations of stirred tanks and associated process equipment has been attempted previously. Investigations have primarily been focused upon two-phase solid–liquid systems, to attempt to replicate experimentally obtained statistics. These simulations have successfully predicted the hydrodynamics and the distributions of the residence and circulation times (Wadnerkar et al., 2012; Jadhav and Barigou, 2022), with Lagrangian particles typically being used to represent the solid phase. In simulations of single-phase or two-phase gas–liquid systems, particle tracking has been used to provide additional insights into hydrodynamic flow structures (Aubin and Xuereb, 2006; Arlov et al., 2008; Kuschel et al., 2021) as well as a unique insight into the lifelines of biological cells in a stirred tank system (Haringa et al., 2016).

1.2. Péclet number

To better understand the transport mechanisms governing mixing in stirred tanks, several studies have adopted approaches based on the fundamentals of a Péclet number, comparing the convective and dispersive transport behaviours within a given system (Bremer and Turek, 2024). For single-phase systems, approaches have quantified the relative contributions of impeller-driven bulk convection and turbulence-induced dispersion through local or global Péclet numbers (Patwardhan, 2001). In aerated stirred tanks, modified forms have been proposed, such as by Montante and Paglianti (Montante and Paglianti, 2015), who displayed the results as an "inverse modified Péclet number". In this representation, positive values indicate increasing dominance of axial dispersive transport generated by the impeller induced-turbulence and larger-scale recirculation. Conversely, negative values arise when operating below the flooding transition point, reflecting

Table 1
Some correlations in literature for the mixing times in two-phase gas–liquid stirred tank reactors.

Author	Correlation	Notes
Cooke et al. (Cooke, 1988)	$\theta_{90} = \frac{3.3}{N_p^{1/3} N \left(\frac{D}{T}\right)^{2.43}}$	Correlation for θ_{90} (90% mixing time)
Vasconcelos et al. (Vasconcelos et al., 1995)	$\theta_{95} = 2.3\exp\left(0.83 n_i + \frac{0.68T}{D}\right)$	Correlation for a multiple impeller system (n_i is number of impellers)
Zhao et al. (Zhao et al., 2001)	$\theta_{95} = 5.9 T^{2/3} \varepsilon_T{}^{-1/3} \left(\frac{T}{D}\right)^{1/3}$	Correlation is a modification of the single-phase mixing time proposed by Ruszkowski.
Shewale and Prandit (Shewale and Pandit, 2006)	$\theta_{95} = 453.7 U_{SG}^{0.127} + 583.95 \left(\frac{H_s \varphi_g}{T}\right)^{-0.496} \left(\frac{P_{IG}}{P_{IU}}\right)^{-0.39} Fr^{0.858} Ri^{0.294} N^{-1}$	Correlation for a dual impeller system (fitted with one PBTD and one RT). (Ri is the Richardson number)

convection dominated behaviour associated with a bubble rise, rather than implying physically negative dispersion.

More recently, Zak et al. (Zak et al., 2025) applied a gas-phase Péclet number derived from axial dispersion modelling of the gas residence time distribution. This Peclet number was used to quantify differences between ideal mixing conditions and the experimentally measured conditions under various operating configurations. These frameworks have been successfully applied to single-impeller (Montante and Paglianti, 2015) and multiple-impeller (Zak et al., 2025) aerated systems, enabling complex hydrodynamic behaviour and mixing mechanisms to be reduced to a single scalar value.

1.3. Lagrangian measurement approaches

The above review of the literature identifies scope for a high resolution, non-invasive measurement technique which can be applied to stirred vessels containing opaque fluids and/or high gas volume fractions, to obtain hydrodynamic data. Nucleonic measurements have been exploited to fill this gap. These include Computer-Activated Radioactive Particle Tracking (CARPT) (Rammohan et al., 2001; Khopkar et al., 2005; Guha et al., 2007) and Positron Emission Particle Tracking (PEPT) (Parker et al., 1993), the technique employed in this study. PEPT is a non-invasive, nucleonic, three-dimensional Lagrangian measurement technique and it has been used to interrogate laboratory-scale stirred tanks with single-phase fluids (Fangary et al., 2000; Chiti et al., 2011), two-phase solid–liquid (Guida et al., 2009; Guida et al., 2010), two-phase gas–liquid (Fishwick et al., 2005; Peace et al., 2025) and three-phase gas–solid–liquid (Fishwick et al., 2003; Cole et al., 2022) systems. To obtain PEPT data, a small tracer particle is radioactively labelled with a radioactive isotope, typically Fluorine-18 (^{18}F), Sodium-22 (^{22}Na) or Gallium-68 (^{68}Ga) (Windows-Yule et al., 2020), and inserted into the experimental system. The radioactive particle undergoes β^+ decay, emitting multiple pairs of highly penetrating gamma rays, with each pair being anti-parallel and colinear in nature to within $\pm 0.5^\circ$ (Windows Yule et al., 2021). Detection and triangulation of these events enable the particle position and thus the particle trajectory to be obtained as a function of time. By using specially developed algorithms (Windows Yule et al., 2021), particle positions can be resolved with sub-millimetre accuracy at particle velocities of approximately $1 - 1.4$ m s^{-1} (Windows-Yule et al., 2020; Windows Yule et al., 2021; Parker et al., 2002). PEPT studies to date have focused on obtaining hydrodynamic data based on either the Lagrangian trajectories or via analysis to convert into a Eulerian dataset for validation of CFD studies (Liu and Barigou, 2013; Hart-Villamil et al., 2024).

In this paper, Lagrangian PEPT data is used solely for the first time to determine mixing times. Whilst Lagrangian data from other measurement techniques have been used to assess fluid circulation, mixing times have been calculated using alternative measurement techniques e.g. decolourisation (Hofmann et al., 2025). The method used for assessing mixing time in this study is the quantity of 'Dispersion', initially proposed for PEPT data by Martin et al. (Martin et al., 2007). In their work, this was applied to PEPT data collected from a fluidised bed, high shear granulator and a small, bladed solids mixer. By analysing the variance in the particle trajectories from a loosely grouped location, from an arbitrary start time ($t = t_0$) to some subsequent time ($t_1 = t_0 + \Delta t$), the efficiency of the mixing device was quantified using a metric named 'Mixing Effectiveness' (ME). This allowed for a quantitative evaluation of the local and global mixing behaviour.

Bashiri et al. (Bashiri et al., 2016) proposed a Lagrangian approach to mixing time estimation using Radioactive Particle Tracking (RPT), based on the statistical decorrelation of particle trajectories. Two indices were used: a 'weak sense' mixing index, derived from the correlation between initial and final positions of segments of a single-particle trajectory, and an autocorrelation-based approach that defines mixing time as the point where the trajectory memory loss occurs, indicated by the autocorrelation values falling within specified confidence intervals. Whilst this method is robust, this approach focuses more on the temporal independence rather than the physical dispersion of the tracer particle.

Hofmann et al. (Hofmann et al., 2025) used Lagrangian particle trajectories from a 40 mm diameter "Lagrangian Sensor Particle – LSP" to determine particle circulation times in a large-scale model of an industrial bioreactor. The LSP was shown to be able to resolve flow structures at the meso-to macro scale at length scales greater than the size of the impeller, based on a Stokes number analysis. Their work focused on a bespoke design, high aspect ratio, 15,000 L bioreactor equipped with multiple impellers under in single-phase and two-phase aerated conditions. Calculation of a 95% mixing time via the LSP data was not attempted, however their work identified a ratio between 95% mixing time calculated from decolourisation experiments and overall circulation time from the LSP measurements with a Rushton turbine, ranging between 2.6 and 4, in line with literature results (Bisgaard et al., 2021). Their mixing time data was in good agreement with a modified form of Eq. (1) presented by Cooke et al. (Cooke, 1988) amongst others.

1.4. Purpose of investigation

The literature reviewed above shows that whilst mixing times, obtained from using another method such as decolourisation, have been correlated to particle circulation times obtained using Lagrangian statistics, mixing times have not been directly determined before solely using Lagrangian particle statistics.

Using the Lagrangian statistics from PEPT experiments, we present and validate a methodology for the quantification of mixing time without relying on optical access for the capturing of a tracer dispersion, or the use of invasive local probe measurements. The whole-field, time resolved view of the mixing behaviour afforded by the Lagrangian data captures local heterogeneities which provides an additional level of robustness to the mixing characterisation.

The methodology is first validated in a series of single-phase experiments containing Newtonian media, with the results from the Lagrangian-based method being compared to well-established empirical correlations in literature as well as an optical-based decolourisation technique. Next, the non-optical nature of the PEPT technique is exploited by measuring the mixing times in highly aerated stirred tank systems involving Newtonian and non-Newtonian media across both the flooded and dispersed aeration regimes. The aeration rates, in terms of superficial gas velocities and volumetric flow rates as a function of the overall tank volume, are representative of industrial practice, but remain poorly characterised due to limitation of conventional measurement approaches. The chosen operating conditions for the non-Newtonian cases are appropriate for the typical operating conditions experienced within industrial production processing of viscous non-Newtonian media, such as those encountered in the fermentation of filamentous fungi (Gabelle et al., 2012; Hardy et al., 2017). Given the high viscosities of these mixtures, the systems would be operating within the transitional flow regime, as studied in this investigation. It remains an open question whether established mixing time correlations, originally developed for single-phase systems and somewhat cautiously extended to two-phase gas–liquid systems containing low gas fractions and Newtonian fluids, remain valid under such industrially relevant operating conditions.

By comparing the PEPT-derived mixing times with existing theory, including both classical mixing time correlations and the relationship between mechanical dispersion and bubble-induced advection, this study addresses a key gap in the understanding of gas–liquid mixing performance at industrially relevant gas loadings.

2. Materials and methods

2.1. Operating conditions and dataset

Experiments were conducted in a flat-bottomed tank of diameter T =

0.2 m; a schematic is shown in Fig. 1. Four longitudinal baffles of width T/10 were fitted flush to the tank wall, spaced every 90°. The tank was filled up to a height H = T, resulting in a working fluid volume of 6.283 L. To enable comparison of results between radial and axial mixing patterns, experiments were performed with either a standard radial pumping Rushton turbine (RT) (Rushton et al., 1950) of diameter D = T/3 and clearance height C = T/3, or an axial pumping 60-degree up-pumping pitched-blade turbine (PBTU) of diameter D = 0.4 T and a clearance height of C = 0.36 T. The chosen dimensions of the impellers fall within the standard dimensions for these impeller types (Paul et al., 2004). For all the aerated cases, a ring sparger of diameter d = T/4 was positioned centrally on the vessel axis, at a clearance height c = T/6. The sparger contained 13 holes, each of 1 mm diameter, with a 5 mm diameter pipe connecting the sparger ring to the top of the tank, where it was connected to the external compressed air supply. This pipe was routed close to a baffle to prevent interference on the flow field.

The experimental conditions used are given in Table 1. Gas was supplied via a compressed air supply and regulated using a Bronkhorst MASS-STREAM D-6371 mass flow controller and a personal computer with bespoke Python code. In aerated cases, gas flow rates (Q_G) of 10.05, 18.89 and 31.42 L min^{-1} ($Q_G = 1.68 \times 10^{-4}$, 3.14×10^{-4} and 5.24×10^{-4} m^3 s^{-1}) were used, corresponding to superficial gas velocities (U_{SG}) of 0.53, 1.00 and 1.67 cm s^{-1} and volumetric flow rates (Vessel Volumes per Minute) of 1.6, 3.0 and 5.0 respectively. The superficial gas velocities and volumetric flow rate (VVM) were selected to fall within ranges that are typical of larger-scale industrial bioreactors. Newtonian experiments utilised a viscous aqueous glycerol solution (70% (v/v) Glycerol) comprising of tap water and Fisher Scientific Glycerol (98+% Extra Pure) ($\rho = 1182$ kg m^{-3}, $\mu = 33.32$ mPa s).

Two solutions of non-Newtonian shear-thinning Sodium Carboxymethylcellulose (CMC) (Ashland CMC-7HF, Ashland, United States) were used, with the powder being mixed with tap water. The density of the CMC solutions was assumed to be approximately 1000 kg m^{-3}, as both polymer concentrations were relatively low (0.5% and 1.0%, both by weight), and the density increase over pure tap water solutions have been shown to be minimal (Cancela et al., 2005).

Fluid rheology was measured using a roughened 40 mm diameter, parallel plate geometry. Both CMC solutions were found to fit a power law rheology model as defined by Eq. (2), with measured values for both solutions as follows: 0.5% (w/w) (K = 390 mPa s^n, n = 0.63) and 1.0% (w/w) (K = 3370 mPa s^n, n = 0.49). For the non-Newtonian cases, apparent viscosities were approximated using the Sánchez-Pérez correlation for average shear rates for turbulent flow in stirred tanks (Sánchez Pérez et al., 2006), shown in Eq. (3). This approach was selected instead of the commonly used Metzner-Otto correlation (Metzner and Otto, 1957), as the Metzner-Otto correlation was developed for flows in the laminar regime and has limited physical meaning outside of this flow regime (Delaplace et al., 2020). The calculated average apparent viscosities, μ_a, of the CMC solutions are shown in Table 2. The apparent viscosities for the 1.0% (w/w) CMC solution are an order of magnitude greater than the apparent viscosities calculated for the 0.5% (w/w) CMC solution for all cases.

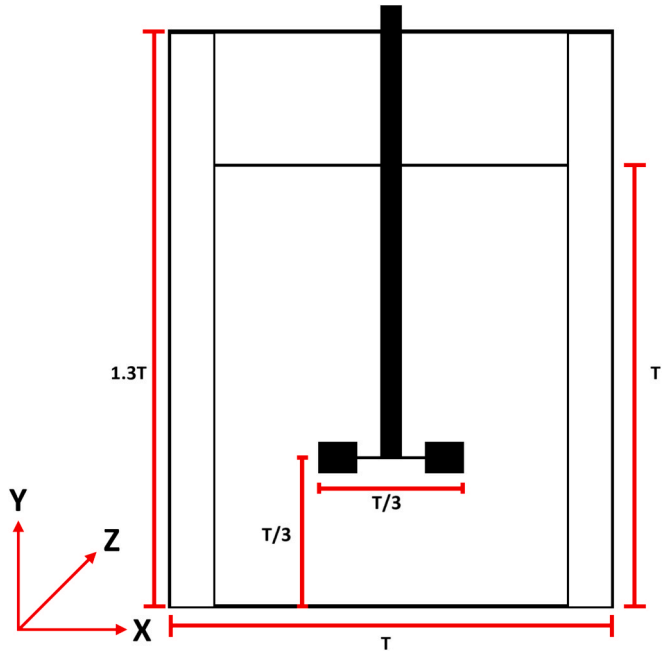

Fig. 1. Schematic of tank setup (single-phase with Rushton turbine).

$$\mu_a(\dot{\gamma}) = K\dot{\gamma}^{n-1} \tag{2}$$

$$\dot{\gamma}_{AVG} = \left(\frac{4\rho N_p D^2}{27K\pi}\right)^{\frac{1}{1+n}} N^{\frac{3}{1+n}} \tag{3}$$

2.2. Power input (Torque)

Power input was obtained via torque measurements on the impeller shaft using a SGR520 torque transducer (Sensor Technology Limited, Banbury, UK). Three measurements were undertaken for a duration of 180 s, in both single- and two-phase operating conditions. Additional measurements were undertaken without fluid, to determine the losses due to mechanical drag from the motor and the bearings. This enabled the torque due to the transfer of mechanical energy into the fluid to be determined. The measured power values and the derived power numbers for all single-phase Newtonian cases are shown in Table A in the Supplementary Information. Impeller contributions for the two-phase Newtonian and non-Newtonian cases are shown in Tables B and C respectively in the Supplementary Information.

2.3. Gas hold-up/void fraction

The average global gas hold-up for each aerated case was determined through triplicate visual measurements of the fluid free surface expansion height (ΔH) and comparing it to the original fluid height (H). The percentage gas hold-up / void fraction, ϕ_g, was calculated using Eq. (4), with the associated void fractions for each case being shown in Table 2.

$$\phi_g = 100 \times \frac{\Delta H}{H + \Delta H} \tag{4}$$

2.4. PEPT measurements

PEPT experiments were performed at the University of Birmingham's Positron Imaging Centre, using the ADAC Forte PET camera (Parker et al., 2002). The tracer particle used was a single ion exchange resin particle of diameter $d_p = 300$ μm and of density $\rho_p = 1182$ kg m^{-3}. The particle was deemed to be neutrally buoyant in the aqueous Newtonian solution by performing an experiment where the motion of the particle was observed in a volume of static fluid for two hours, with no motion of the particle being observed. In the CMC solutions, a small density difference was present to aid the particle in its transit out of any stagnant flow zones in the vessel. Stokes numbers, *Stk*, for this particle under single-phase Newtonian conditions were calculated to be in a range of $0.0018 < Stk < 0.0071$, using Eq. (5). Previous studies using PEPT have determined that if Stk < 0.01, the particle can be deemed as a true velocimeter (Guha et al., 2007; Guida et al., 2009; Guida et al., 2010), and therefore faithfully follow the flow for all cases.

$$Stk = \frac{\tau_p}{\tau_f} = \frac{\rho_p {d_p}^2}{18\mu_a} \frac{D}{U_{TIP}} \tag{5}$$

Table 2
Experimental operating conditions, apparent viscosities and gas void fractions.

Condition	Impeller	N [RPM]	Re [-]	Fr [-]	U_{SG} [cm s^{-1}]	Fl_G	μ_a [mPa s]	φ_g
Newtonian Single-Phase	RT	190	500	0.07	0.00	0.00	33.3	N/A
		301	800	0.17				
		393	1030	0.29				
		530	1400	0.53				
		667	1750	0.84				
		764	2000	1.10				
	PBTU	300	1135	0.20	0.00	0.00	33.3	N/A
		500	1890	0.57				
Newtonian Two-Phase (Flooded)	RT	190	500	0.07	0.53	0.18	33.3	0.5%
					1.00	0.34		1.0%
					1.67	0.56		2.5%
Newtonian Two-Phase (Dispersed)	RT	530	1400	0.53	0.53	0.06	33.3	1.0%
					1.00	0.12		2.5%
					1.67	0.20		4.0%
	PBTU	300	1135	0.20	0.53	0.07	33.3	1.5%
					1.00	0.12		2.0%
		500	1890	0.57	0.53	0.04	33.3	3.0%
					1.00	0.07		4.5%
0.5% CMC Two-Phase (Dispersed)	RT	621	675	0.73	0.53	0.05	81.9	3.5%
					1.00	0.10	82.3	2.0%
		1306	2300	3.22	0.53	0.03	52.6	2.0%
					1.00	0.05	52.9	3.5%
1.0% CMC Two-Phase (Dispersed)	RT	1306	280	3.22	0.53	0.03	710	4.0%
					1.00	0.05	756	6.5%
					1.67	0.08	763	9.0%

The resin particle was doped with Fluorine-18 (^{18}F) in water, with a resin lacquer then applied to seal the ^{18}F ions into the particle and then inserted into the experimental system. ^{18}F was chosen due to its short half-life of 109.8 min (Alauddin, 2012), meaning it was relatively easy to store and dispose of. As the particle traverses the system, β^+ decay occurs, emitting positrons which annihilate with nearby electrons in the surrounding fluid media, resulting in the emission of a pair of co-linear 511 keV gamma rays. As tens of thousands of gamma ray pairs are emitted per second, their position can be triangulated to obtain particle positions over time at a high frequency in the order of 10^3 Hz. Because PEPT is a single particle tracking technique, it is necessary to perform each measurement for a suitable duration to ensure ergodicity of the statistics. In the present work, data are taken for a minimum duration of 3 h, comfortably more than the requirement for ergodicity (Guida et al., 2009; Chiti et al., 2011). The positions of the tracer particle were determined using the PEPT-ML algorithm (Nicuşan and Windows-Yule, 2020), with the instantaneous velocities calculated via the use of a two-dimensional, seven-point fitted, moving polynomial approach. Lagrangian statistics are outputted at a fixed time step of 5 ms, equivalent to a sampling rate of 200 Hz, in Cartesian co-ordinates and located in the global co-ordinate system of the PEPT scanner. These positions were normalised with respect to the tank diameter, T, and subsequently converted to polar co-ordinates.

2.5. Mixing times via PEPT measurements

Each dataset comprised a single, continuous Lagrangian trajectory of the radiolabelled particle tracked via PEPT. The trajectory was segmented into a series of shorter sub-trajectories, allowing the statistical properties to be calculated locally from the repeated transits through each voxel. As the statistics were ergodic in nature, this allows for the single-particle trajectory to yield spatially resolved mixing information. Based on the methodology developed by Martin et al. (Martin et al., 2007), a cylindrical grid was formed equal to the size of the fluid region, with each voxel being of equal volume. Calculations using the 'mixing effectiveness' (ME) metric were performed using the Up[4] open-source software package (Werner, 2022).

To evaluate the reliability of the Lagrangian mixing time measurements to the voxel size tests were performed with 10, 20 and 40 voxels in each of the radial (r), axial (y) and azimuthal (θ) directions, (corresponding to 1,000, 8,000 and 64,000 total voxels respectively). 10 voxels per direction resulted in significantly under-estimated dispersion, due to the larger voxels obscuring the smaller scale motion of the particle throughout the system. 40 voxels were found to show substantial noise and was not consistently able to converge on a solution due to the over-segmentation of the domain. Based upon these findings, a resolution of 20 voxels per direction was selected as an appropriate compromise, offering both numerical stability and sufficient spatial resolution to capture the relevant fluid and particle dynamics. Small changes about this value did not materially change the values of the measured particle dispersion. Dispersion statistics were obtained within each voxel only when more than one particle sample contributed ($n > 1$). Although individual voxel contributions may be subject to local variability, the > 3 h acquisition time per experiment considerably exceeds the durations previously reported to obtained statistically ergodic behaviour in comparable previous PEPT investigations (Chiti et al., 2011). The large ensemble of overlapping trajectory samples, evaluated at each valid time step, ensures that there was statistical convergence of the mixing effectiveness metric at the selected spatial resolution.

In this investigation, a value of Δt of 20 ms is used. This choice mirrors the 50 Hz sampling rate typical of optical-based methods, enabling consistency with benchmark techniques. Varying the time step between 20 ms and 80 ms showed negligible influence on the computed mixing time. While coarser time steps introduced greater percentage uncertainty, the absolute values of dispersion were stable, indicating that the method is not inherently dependent on the temporal resolution. Each measurement was performed for a duration of 12 s (12000 ms), to ensure a steady-state value of ME was obtained across the full range of

system parameters explored. The dispersion calculation is performed at each time step, corresponding to a highly overlapped sampling strategy with an effective spacing between each successive trajectory being equal to the sampling frequency of the PEPT experiments (5 ms, 200 Hz). Therefore, a large ensemble of start points was obtained for each dataset.

As the tank is axisymmetric, a modified version of the equation proposed by Martin et al. (Martin et al., 2007) is used, where the azimuthal component is averaged. This approach is justified as variations in the azimuthal direction are negligible when compared to variations in the radial and axial directions.

Firstly, the particle dispersion is computed by integrating on a voxel-by-voxel basis in the PEPT measurements using Eq. (6) (Martin et al., 2007).

$$\sigma^2 = \frac{1}{n_v}\sum_{i=1}^{n_v}(r_i - \bar{r})^2 + (y_i - \bar{y})^2 \tag{6}$$

where σ^2 is the variance of the particle position (a measure of the particle spread from a loosely grouped region, with units of length^2), i is the index of the voxel which the calculation is referring to, r_i and y_i to the r and y positions of the i^{th} voxel, $\bar{r}$, and $\bar{y}$ are the mean positions of the particles in the r and y co-ordinates, respectively and n_v is the number of voxels to describe the system.

The variance of the particles is then used to calculate the mixing effectiveness (ME, mm^2) of the system (Martin et al., 2007), shown in Eq. (7), where $n_{p,i}$ is the number of passes from the particle through each i^{th} voxel, weighting the mixing on a voxel-by-voxel basis based upon the number of passes of the particle through a given voxel. Owing to the constant voxel volume discretisation, ME values were computed with no weighting applied for cells close to the tank wall or near the impeller region.

$$ME = \frac{1}{n_p}\sum_{i=1}^{n_v}\sigma^2 n_{p,i} \tag{7}$$

Plotting the change in ME over time yields the curve shown in Fig. 2, with the curve reaching a plateau. The plateau identifies where the variance of the particle positions cannot increase any more due to being constrained by the geometry of the system, i.e. the particles have reached the extremities of the vessel walls and cannot "spread out" from one another any further.

To mathematically identify where the ME reaches a plateau, the first derivative of the ME is taken against time. This is then normalised by the maximum change of the derivative, as shown by Eq. (8).

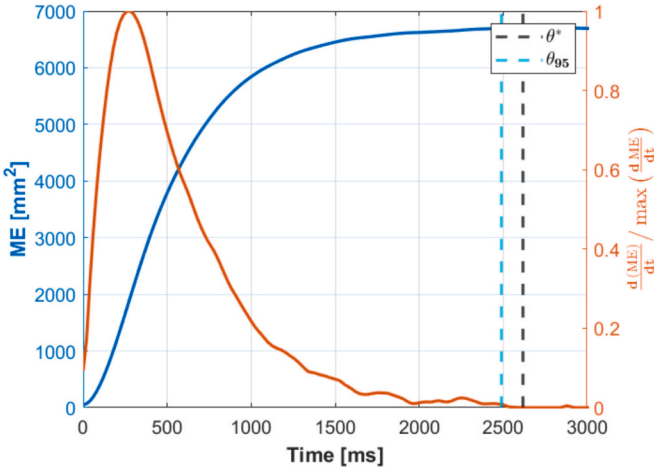

Fig. 2. Graph showing change of ME over time and rate of change of the normalised ME. θ* and θ_{95} marked on the graph. (N = 764 RPM, U_{SG} = 0 cm s^{-1}).

$$\left(\frac{d(ME)}{dt}\right)_{NORM} = \frac{\left(\frac{d(ME)}{dt}\right)}{max\left(\frac{d(ME)}{dt}\right)} \tag{8}$$

Eq. (9) shows the first time where the normalised derivative equals zero. This time, θ^*, was identified as the earliest point where the normalised first derivative equals 0 and substantially remains at 0, as shown by Fig. 2. Due to experimental noise, this determination was assessed by a manual inspection of the local derivative and the derivative curve itself and not using a fixed numerical threshold.

$$\theta^* = min\left\{t \middle| \left(\frac{d(ME)}{dt}\right)_{NORM} = 0\right\} \tag{9}$$

θ_{95} is defined as the time at which the mixing effectiveness reaches 95% of its final value, as described by Eq. (10), with this also being shown in Fig. 2.

$$\theta_{95} = 0.95\theta^* \tag{10}$$

The relationship between mixing effectiveness and mixing time can be understood theoretically by drawing an analogy with classical diffusion. In diffusive systems, the mean squared displacement (MSD) of a tracer is given by Eq. (11), where D_{EFF} is the effective dispersion coefficient.

$$\langle \Delta x^2 \rangle = 2D_{EFF}\, t \tag{11}$$

In this context, ME is a spatially averaged measure of the particle variance, calculated from repeated trajectory segments emanating within each voxel. Since it captures the extent of particle spreading over time, ME scales similarly to the MSD. In the early stages of the mixing process, this gives Eq. (12):

$$ME(t) \sim D_{EFF}\, t \tag{12}$$

If we define the mixing time, θ_m, as the time required for the tracer to fully explore the system, it can be approximated by the time required for the particle to spread across a characteristic length scale. For a stirred tank, a natural choice for this length scale is the tank diameter, T. Therefore, the mixing time can be written as Eq. (13). Substituting the relation developed in Eq. (12) gives Eq. (14).

$$\theta_m \sim \frac{T^2}{D_{EFF}} \tag{13}$$

$$\theta_m \sim \frac{T^2 t}{ME(t)} \tag{14}$$

This shows that, for a given tank size and an observation time, t, the mixing time is inversely proportional to the ME. This relationship assumes two key conditions: the system is in a statistically steady state and the particle trajectory, and therefore the data obtained, is ergodic in nature. These assumptions are valid here due to the 3 hour acquisition time and the well-developed, steady-state flow field in the stirred tank. Under these conditions, ME serves not only as a spatial indicator of mixing performance, but also as a robust proxy for determining mixing times in cases where direct scalar measurements are not possible.

2.6. Mixing times via acid-base decolourisation (ABD)

The acid-base decolourisation technique employed uses the methodology from Cabaret et al. (Cabaret et al., 2007). A fast acid-base reaction between hydrochloric acid (HCl) and sodium hydroxide (NaOH) is conducted within the tank in the presence of bromocresol purple (BP) (1.6×10^{-5} M), a pH indicator, which appears purple at pH > 6.8 and yellow at pH < 5.2. The colour changing nature of BP is leveraged to evaluate mixing inside the tank. First, the bulk fluid is set a deep red

colour via dropwise addition of 10 M NaOH and the volume of 10 M HCl required to turn the solution yellow is determined experimentally (0.04 mL). An acid-to-base ratio greater than 2:1 is recommended to ensure repeatable macromixing times are attained in decolourisation experiments (Godleski and Smith, 1962), so 0.1 mL of HCl is diluted into 0.9 mL of bulk solution to create an acidic premix. The premix has similar viscosity and density to the bulk fluid to reduce their impact on the mixing process.

Mixing inside the tank is, thus, evaluated by depositing the acidic premix at a fixed point on the free surface using a wide-nozzle syringe, initiating the colour change from deep red through orange and, finally, yellow. The process is filmed and digitally analysed based on RGB-based criteria to extract θ_{95}. After the run has finished, 0.1 mL of NaOH is added to the tank to reset the colour to deep red before removing 1.1 mL to maintain a constant volume inside the tank.

A typical evolution of the colour inside the tank via the acid-base decolourisation technique is shown in Fig. 3.

Each mixing run was recorded using a Fujifilm X-T3 mirrorless camera at a resolution of 1080p and frame rate of 25 fps, recording until the fluid appeared uniformly yellow or until a 10-minute cut-off time was reached. Optical distortions due to curvature of the tank walls were minimised by placing the vessel inside a rectangular acrylic viewing box, filled with water, which was backlit by an LED panel (Gekko Karresslight 6006). To ensure that mixing was run until completion, the green channel pixel intensities were evaluated and checked for stabilisation during post-processing. Triplicate experiments were performed to eliminate any anomalous mixing time statistics.

The mixing recordings were exported as MOV files and converted into series of PNG images for quantitative evaluation of mixing time. Before processing, these images were masked to exclude the tank walls, impeller, shaft and any free surface deformation from the analysis. This allowed for the bulk flow of the system to be focused on. A custom Python script was written to extract θ_{95} from these masked image series, working with arrays of green channel pixel values, G, extracted from each frame. This channel was selected because it most accurately represents the change in colour seen in decolourisation experiments using BP (Cabaret et al., 2007; Delbridge et al., 2023).

For each frame, a normalised signal intensity, G', was calculated on a pixel-by-pixel basis using averaged initial, G_0, and final, G_∞, signal values, and as per Eq. (15). Averaged arrays were employed to account for variation in G due to LED backlight flicker, using the first and last 10 frames for G_0, and G_∞ respectively.

$$G' = \frac{G - G_0}{G_\infty - G_0} \tag{15}$$

Since each pixel could be treated as an individual probe, the root mean square variance of G', σ_{RMS}, for each frame was calculated as per Eq. (16) (Paul et al., 2004), where N_{px} is defined as the number of non-masked pixels in the image.

$$\sigma^2_{RMS} = \frac{1}{N_{px}} \sum_{i=0}^{n} (G' - 1)^2 \tag{16}$$

The 95% mixing time, θ_{95}, was defined as the time required for the green-channel pixel intensity extracted from the RGB images, as discussed prior, to reach 95% of the total change between the initial unmixed state and the fully mixed steady-state condition, according to the method presented in Delbridge et al. (Delbridge et al., 2023). The value of the 95% mixing time was then identified by visually inspecting the gradient of the log-variance signal. Using the gradient at the point of maximum descent, a linear fit was applied. The mixing time was calculated as the point where this line crossed the threshold value of $\log(0.05) = -2.602$, which corresponded to θ_{95}. This approach was chosen over directly using the log-variance curve, which often exhibits an initial lag phase, similar to the lag effects observed in pH probe-based mixing time measurements, which can significantly skew the measured mixing time of the system (Zhang et al., 2014). The extrapolated time was then compared to the point of closest intersection with the original curve, showing good agreement.

3. Results and discussion

3.1. Validation of Lagrangian mixing times via single phase measurements

To evaluate and validate if the novel measurement methodology proposed can accurately determine mixing times, investigations were made using a series of single-phase systems, containing Newtonian media. Acid-base de-colourisation (ABD) experiments were also performed to provide an independent assessment of the Lagrangian measurement technique using the exact system geometry and fluid properties. These experiments were performed using the methodology described in § 2.5.

Fig. 4 compares the measured values of θ_{95} for Newtonian single-phase flow using the Lagrangian and ABD techniques, along with the benchmark empirical correlation of Grenville (Grenville, 1992), using the RT and PBTU impellers respectively. Good agreement is obtained for all datasets, with the values obtained from all three methods fitting within the error bars, apart from at the lowest impeller speed used with the Rushton turbine (190 RPM). This can be attributed to the reduced

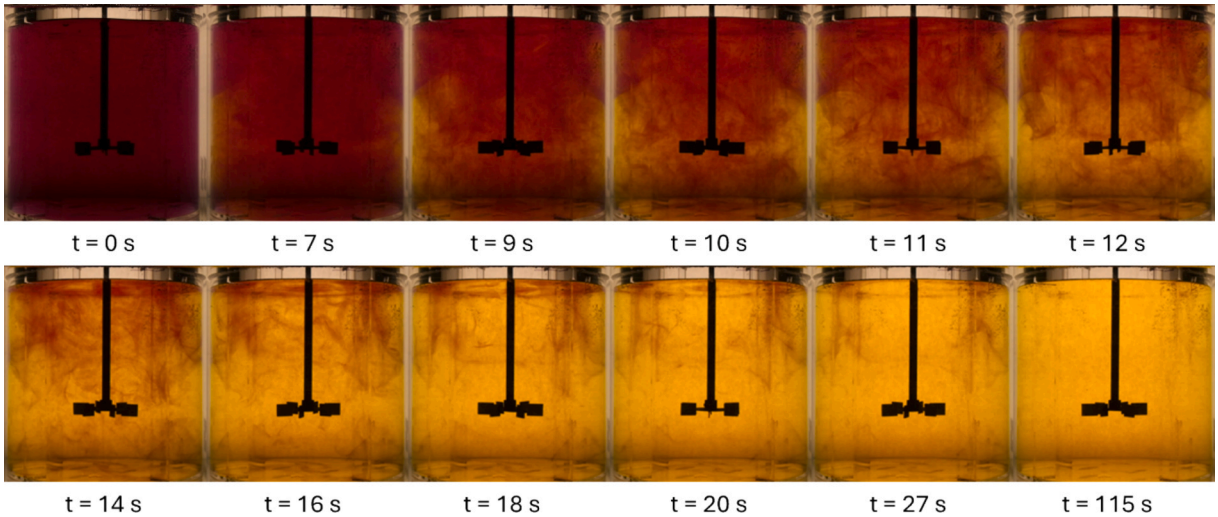

Fig. 3. Typical example of the evolution of mixing with the Rushton turbine using acid-base decolourisation experiments (N = 190 RPM, U_{SG} = 0 cm s^{-1}).

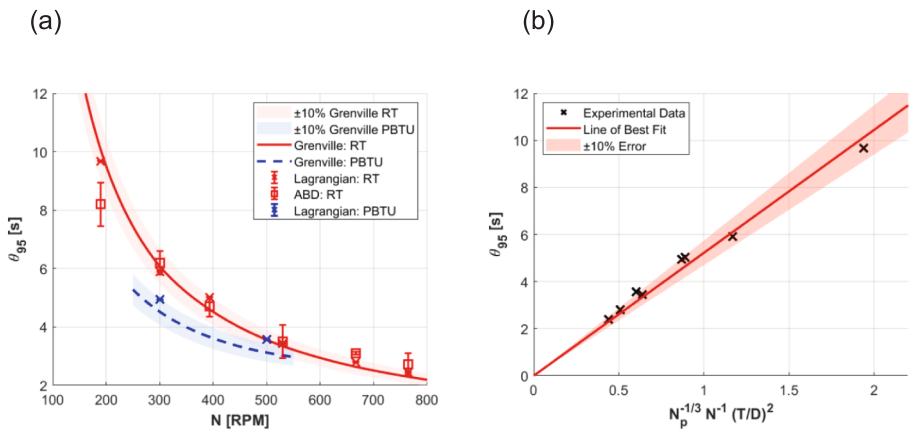

Fig. 4. (a) Comparison of (θ_{95}) values from Lagrangian, empirical (Grenville, 1992) and ABD measurements for single-phase Newtonian experiments. (b) Fit of θ_{95} obtained from Lagrangian measurement versus $\mathbf{N_p}^{\frac{-1}{3}}\mathbf{N}^{-1}\left(\frac{\mathbf{T}}{\mathbf{D}}\right)^2$ – gradient of the solid straight line is the coefficient A of the equation.

turbulence and limited fluid circulation in the vessel at low Reynolds numbers ($Re = 500$), leading to the acid-base reaction occurring more rapidly in the region closest to the injection point. In contrast, the Lagrangian technique matched the mixing times determined through the Grenville correlation across the full range of parameters tested.

The value of coefficient, A, as shown in Eq. (1), was calculated through the Lagrangian mixing effectiveness technique as 5.2 ± 0.5 with an error defined as $\pm$ 10%, matching that of Grenville (Grenville, 1992) and quoted in the later work by Nienow (Nienow, 1997). Whilst the dataset used here is extremely limited compared with that used to generate Grenville's correlation, such good agreement is nevertheless highly encouraging and shows that this analysis obtains values of mixing time equivalent to existing methods.

3.2. Lagrangian mixing times in gas–liquid systems

The PEPT technique enables full field, three-dimensional measurements in opaque systems. Therefore, it is exploited in this work via measurements over a wide range of gassing rates, leading to gas void fractions from 0.5 to 9% in Newtonian and non-Newtonian fluids, as shown in Table 1.

In an aerated vessel, the total power, P_T, has contributions from both the mechanical input due to the rotation of the impeller, P_I, and buoyancy driven effects from the gas flow, P_G. Previous literature has used two different equations for quantifying the contribution due to P_G. Work by Zhao et al. (Zhao et al., 2001) defined P_G by using the gas flow rate (Q_G) and the submergence height of the sparger (H_S). Thus, in this work, $H_S = \frac{5T}{6}$ is used. Eq. (17) is used to calculate the total power in the system.

$$P_T = P_I + \rho_L Q_G H_s g \tag{17}$$

Zhao et al. (Zhao et al., 2001) identified that the single-phase mixing time correlation of Ruszkowski (Ruszkowski, 1994), shown in Eq. (18), fitted their measured mixing time data accurately. The only modification made was using the total specific power ($\varepsilon_T = \left(\frac{P_T}{\rho V}\right)$) instead of using the power supplied by the impeller alone (P_I).

$$\theta_{95} = 5.9 T^{2/3} {\varepsilon_T}^{-1/3} \left(\frac{T}{D}\right)^{1/3} \tag{18}$$

3.2.1. Modified Péclet number

The use of a Péclet number allows for an understanding of the mechanisms (impeller-driven versus buoyancy-driven) of mixing within

Table 3
Bubble rise velocities and calculation of the inverse modified Péclet number for Newtonian and non-Newtonian gas–liquid flow.

Fluid	Impeller	Aeration Regime	U_{SG} [cm s^{-1}]	U_B [cm s^{-1}]	1/Pe*
70% (v/v) Glycerol	RT	Flooded (190 RPM)	0.53	106.00	−0.01
			1.00	100.00	−0.01
			1.67	66.80	−0.02
		Dispersed (530 RPM)	0.53	53.00	0.03
			1.00	40.00	0.02
			1.67	41.75	0.01
	PBTU	Dispersed (300 RPM)	0.53	35.33	0.03
			1.00	50.00	0.02
		Dispersed (500 RPM)	0.53	17.67	0.13
			1.00	22.22	0.10
0.5% (w/w) CMC	RT	Dispersed (621 RPM)	0.53	15.14	0.12
			1.00	50.00	0.03
		Dispersed (1306 RPM)	0.53	26.50	0.22
			1.00	28.57	0.19
1.0% (w/w) CMC	RT	Dispersed (1306 RPM)	0.53	13.25	0.45
			1.00	15.38	0.36
			1.67	18.56	0.27

a given aerated stirred tank system. As discussed in §1.2, the work of Montante and Paglianti (Montante and Paglianti, 2015) defined the relationship between the impeller-driven and gas-driven aspects of the stirred tank system by using a modified Péclet number, as shown in Eq. (19). The axial dispersion coefficient, a measure of the effectiveness of the impeller under aerated conditions, D_I, was calculated using Eq. (20), with an impeller-specific constant, a, equal to 0.16 for a Rushton turbine and equal to 0.12 for an up-pumping pitched-blade turbine (Montante and Paglianti, 2015), with N being the impeller speed. The variable N_{FL} represents the impeller speed at which the transition to the flooded aeration regime is achieved, for a given superficial gas velocity. For the cases with the Rushton turbine, the impeller speed at which the flooding transition occurs was calculated using the correlation, $Fl_G = 30Fr\left(\frac{D}{T}\right)^{3.5}$ (Nienow et al., 1985), comprising the gas flow number (Fl_G), $Fl_G = \frac{Q_G}{ND^3}$, and the impeller Froude number (Fr), $Fr = \frac{N^2D}{g}$, to determine the critical transition point. In the cases involving the up-pumping pitched-blade turbine, the flooding transition speed was calculated by using the correlation, $Fl_G = 6000T^{1.55}Fr^{2.7}$ (Bujalski et al., 1988).

$$Pe^* = \frac{U_B H_L}{D_I} \tag{19}$$

$$D_I = aD^2(N - N_{FL}) \tag{20}$$

The bubble rise velocity, U_B, was estimated using the ratio between the superficial gas velocity, U_{SG}, and the global gas void fraction of the system, shown in Eq. (21). This method was chosen compared to others in literature (Colombet et al., 2015), which require an additional measurement or suitable estimation of the bubble rise velocity at the outlet of each of the sparger holes. This is a challenging measurement to take via image processing techniques in an aerated stirred tank due to accumulation of bubbles at the tank wall. By relating the U_{SG} to the local gas hold-up, this provides a representative swarm velocity that inherently represents the hindrance effects in very dense bubbly flows.

$$U_B = \frac{U_{SG}}{\varphi_g} \tag{21}$$

Table 3 shows the calculated bubble rise velocities and the inverse of the modified Péclet number for all two-phase cases investigated. The high bubble rise velocity in the flooded cases indicates the presence of slug-like bubble formation (Jamshed et al., 2018), with the gas rising around the impeller shaft. For all cases in the dispersed aeration regime, the lower speed bubble rise implies smaller diameter bubbles arising from the gas-impeller interaction (Jamshed et al., 2018; Alves et al., 2002), resulting in greater gas hold-up values generally being obtained (Peace et al., 2025).

3.2.2. Newtonian mixing times

Fig. 5a shows the measured mixing times (θ_{95}) using the Lagrangian technique and comparison to the modified version of the Ruszkowski (Ruszkowski, 1994) equation, proposed by Zhao et al. (Zhao et al., 2001), for the aerated systems containing Newtonian media, operating in both the flooded and dispersed aeration regimes, agitated by either a Rushton turbine or up-pumping pitched blade turbine. In the flooded aeration regime, there is a significant discrepancy in the mixing times between the measured mixing times with the Lagrangian statistics, and the correlation. This can be partially attributed to the very high superficial gas velocities used in this investigation, with much of the power input into the system (approximately 80%) resulting from the gas-driven buoyant motion (Zak et al., 2022), as shown in Table C in the Supplementary Information. When compared to the single-phase case at the same impeller speed and Reynolds number, the mixing times in the flooded regimes are approximately halved.

In the dispersed aeration regime, relatively good agreement is

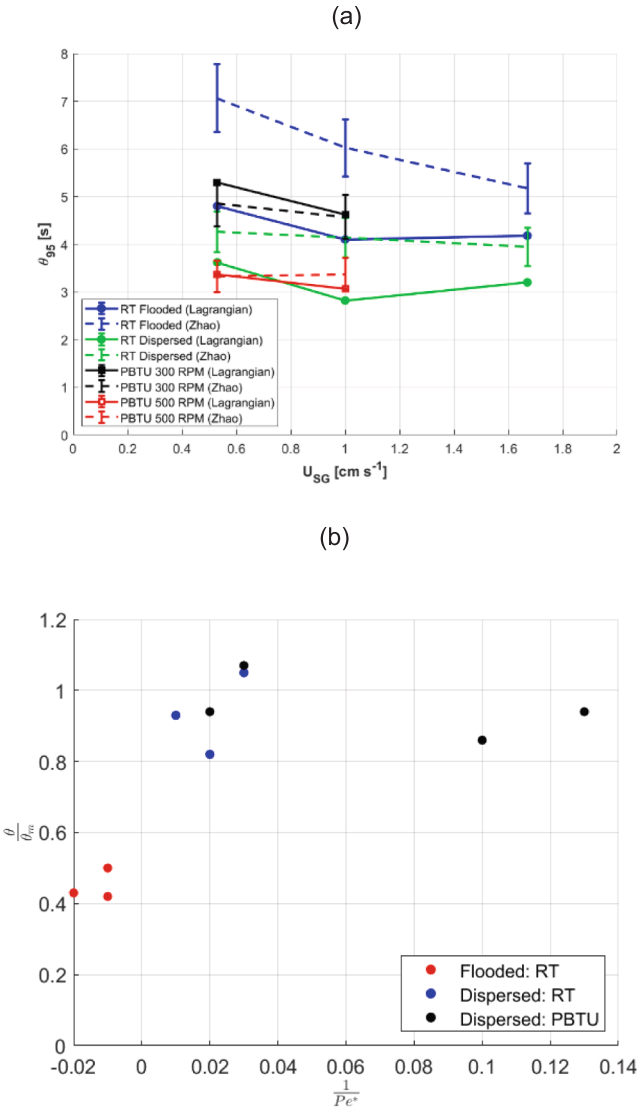

Fig. 5. (a) Measured θ_{95} in two-phase Newtonian systems compared to Zhao et al. (Zhao et al., 2001). (b) Inverse modified Péclet number versus normalised dimensionless mixing time (θ_{95}). $\left(\frac{\theta}{\theta_m}\right)$

obtained with all the cases. The cases with the pitched-blade turbine show an increase in the superficial gas velocity, at a constant impeller speed, decreases the mixing time. On the other hand, in the dispersed cases with the Rushton turbine, an increase in the superficial gas velocity does not necessarily yield a decrease in the mixing times, with the mixing times plateauing at higher superficial gas velocities, matching previously observed behaviour in literature (Zhang et al., 2009; Montante and Paglianti, 2015; Zak et al., 2022). This can be attributed to the poor performance (a significant drop in P_I) of the Rushton turbine under highly aerated conditions, only being partially offset by the additional power inputted by the gas.

Fig. 5b highlights the role of buoyancy-driven circulation relative to the impeller-induced dispersion. In the flooded aeration regime, the normalised mixing time is substantially lower (approximately 0.4 – 0.5), reflecting the strong contribution of the gas buoyancy to the bulk fluid circulation, despite limited mechanically driven dispersion from the impeller. Conversely, in the dispersed aeration regime, regardless of impeller type, the normalised mixing time, the mixing time with respect to the equivalent single-phase case, remains close to 1. This indicates that the gas-phase motion contributes less significantly to an overall

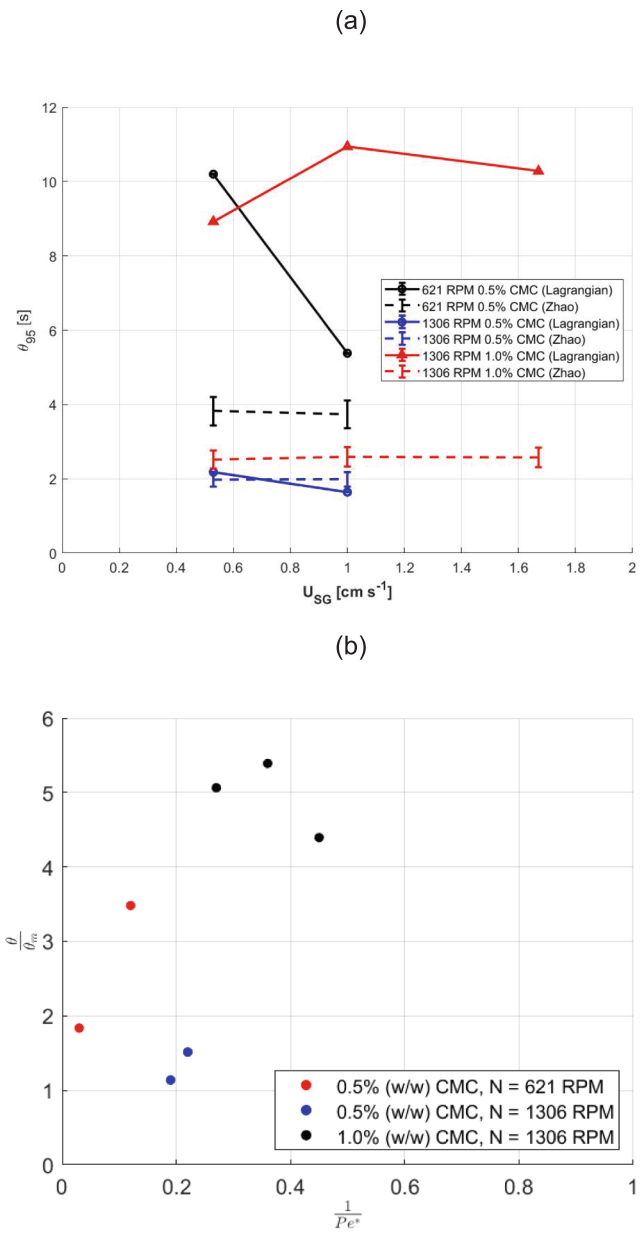

Fig. 6. (a) Measured θ_{95} in two-phase non-Newtonian media compared to Zhao et al. (Zhao et al., 2001). (b) Inverse modified Péclet number versus normalised dimensionless θ_{95} $\left(\frac{\theta}{\theta_\infty}\right)$ for non-Newtonian fluids.

homogeneity of mixing performance once the impeller dispersion is established. Despite the total power input being accounted for in the original correlation, the conditions explored in this work, particularly in terms of the contribution of gas, up to U_{SG} = 1.67 cm s^{-1} (5 VVM), extends well beyond the range investigated in previous studies, taking advantage of the capabilities of PEPT to interrogate opaque systems.

3.2.3. Non-newtonian mixing times

Fig. 6a shows the 95% mixing times for all cases using non-Newtonian 0.5% (w/w) or 1.0% (w/w) CMC solutions, with all operating within the dispersed aeration regime. With all the cases of the 0.5% (w/w) CMC, the mixing time decreases with the increase in the superficial gas velocity. This is significant in the Re = 280 cases, where a 47% decrease in the mixing time is observed between U_{SG} = 0.53 and 1.00 cm s^{-1}. The Zhao correlation (Zhao et al., 2001) predicts the mixing times at Re = 2300 reasonably well but significantly under-predicts the mixing times at the Re = 675. This under-prediction is also observed in all the 1.0% (w/w) cases, with the measured mixing times using the Lagrangian method being approximately 3 – 4 times greater than those predicted with the correlation. A possible explanation is that the correlation was developed for fully turbulent flow regimes in the dispersed aeration regime (Zhao et al., 2001), the flow is in the transitional flow regime and therefore by its nature, are more strongly influenced by the fluid rheology. The higher apparent viscosity of the 1.0% (w/w) CMC solution significantly dampens the turbulence and reduces the effectiveness of gas-induced mixing. Although the data presented here are limited, the large differences observed do highlight a gap in the predictive capability of existing correlations, which can be explored further via full-field Lagrangian measurements.

Fig. 6b illustrates the relationship between the dimensionless mixing time with respect to the inverse modified Péclet number respectively. For the non-Newtonian systems, single-phase reference experiments were not performed using the PEPT or ABD techniques. Instead, the single-phase correlation of Grenville (Grenville, 1992) was used to allow for a consistent baseline for normalisation.

The dimensionless mixing times increase in Fig. 6b show that the presence of gas does not improve the global mixing behaviour inside the non-Newtonian systems. No correlation is apparent between the inverse modified Péclet number and the measured mixing times, suggesting that, despite the limited dataset, the mixing time and the aeration rate could potentially be independent of one another for systems containing non-Newtonian media.

The impact of rheology is also notable to see in Fig. 6b, with the dimensionless mixing times being significantly larger for the cases with the 1.0% (w/w) CMC solution. One interpretation of our results is that at the lower 0.5% (w/w) CMC concentration, gas injection plays a dual role, not only promoting mixing, but also providing a pre-shear effect in the upper part of the vessel. The rising bubbles impart localised shear, which therefore reduces the local apparent viscosity in shear-thinning fluids and in turn enhancing mixing relative to what might be expected based on mechanical agitation alone. This is also shown with the inverse modified Péclet number being closer to zero in all cases compared to the 1.0% (w/w) CMC solution, with this being an important factor at N = 621 RPM.

This behaviour is consistent with observations reported in literature, with bubble-induced pockets of localised high shear and low fluid viscosity being captured computationally near Rushton turbines in power law non-Newtonian fluids (Moilanen et al., 2006). Larger slug-like bubbles are formed at a higher bubble rise velocity, which possess more momentum and therefore impart more shear to the fluid media (Jamshed et al., 2018). Additionally, the average shear rate across the whole fluid volume has been determined to increase with an increase in the gas flow rate (and therefore superficial gas velocity) (Campesi et al., 2009; Buffo et al., 2016). These results could provide a possible explanation of why, at 0.5% (w/w) CMC (N = 621 RPM, Re = 675), the difference between the measured mixing times at U_{SG} = 0.53 cm s^{-1} and 1.00 cm s^{-1} is significant.

In contrast, in the more viscous 1.0% (w/w) CMC solution, the bubble rise velocity is significantly reduced as shown in Table 2, suggesting that smaller diameter bubbles are formed (Alves et al., 2002), possessing less momentum and consequently imparting less shear to the fluid media. As shown with both Fig. 6b, this results in the impeller dominating the mixing dynamics. Under these aerated conditions with non-Newtonian fluids, empirical correlations based on assumptions from Newtonian systems become increasingly unreliable. Given that these correlations are not suitable in capturing the variability of the mixing performance and time across the whole fluid volume resulting from the non-Newtonian rheology, direct measurements of the fluid mixing time across the whole fluid volume are necessary.

Whilst the present study focuses on single-impeller stirred tanks at a laboratory-scale, the proposed methodology is not intrinsically limited to these configurations. At industrial-scale with multiple-impeller

systems, flow fields can be grouped into multiple circulation regions, with spatial heterogeneity associated with each impeller stage. The nature of the Lagrangian statistics can capture zone-specific mixing behaviour and any associated non-uniform mixing behaviour.

Even though mixing times may quantitatively differ with the system scale and complexity, the underlying Lagrangian framework is based upon particle transport remains applicable. Additional considerations such as compartmentalisation may influence local mixing behaviour in multi-impeller systems and should be accounted for in future applications of the Lagrangian methodology.

4. Conclusions

In this investigation, Lagrangian statistics obtained from Positron Emission Particle Tracking experiments have been used to directly determine mixing times inside single- and two-phase gas–liquid stirred tanks. Under single-phase conditions, excellent agreement was achieved between the 95% mixing times measured via the Lagrangian methodology, acid-base decolourisation experiments and established empirical correlations, demonstrating the equivalence of the analysis used.

The proposed Lagrangian mixing effectiveness methodology is particularly advantageous in situations where classical correlations are known to be less reliable, such as in systems with non-Newtonian fluids or in aerated systems. Whilst empirical correlations provide good practical estimates for conventional Newtonian single-phase systems, existing correlations do not fully capture the complexity of these systems. This Lagrangian approach leverages direct full-field trajectory measurements to characterise the mixing behaviour.

The non-optical nature of the PEPT method allowed for whole field investigation of aerated systems at higher gas void fractions than would be possible with conventional optical techniques. In systems with a Newtonian fluid, the Lagrangian methodology produced mixing time estimates broadly consistent with existing empirical correlations in the dispersed aeration regime. For non-Newtonian systems, fluid rheology was shown to exert a profound influence on the global mixing performance. The existing correlations failed to predict mixing times reliably in shear-thinning, non-Newtonian solutions, especially at Reynolds numbers in the lower transitional flow regime. Increasing the apparent viscosity under identical operating conditions (impeller speed and superficial gas velocities), led to mixing times increasing by a factor of 4. These findings highlight the complex and non-trivial nature of mixing in these systems, and the limitations of traditional established correlations.

The interaction between bubble-driven and impeller-driven dispersion was further investigated using the modified Péclet number approach initially used by Montante and Paglianti (Montante and Paglianti, 2015). This demonstrated that aeration has a very limited impact on dispersion in high-viscosity media, whereas it significantly enhances the dispersion in Newtonian fluids. This approach also provided additional insight into the relatively poor performance of the Rushton turbine under aerated conditions, compared to an axial pumping impeller. This reinforces the need for a tailored impeller selection based upon the fluid rheology and gas dynamics inside the system.

CRediT authorship contribution statement

W.J. Peace: Writing – original draft, Visualization, Validation, Methodology, Investigation, Formal analysis, Conceptualization. **D. Khoshdel:** Writing – original draft, Visualization, Validation, Resources, Methodology, Investigation. **L. Gamet:** Writing – review & editing, Supervision. **F. Augier:** Writing – review & editing, Supervision, Project administration, Funding acquisition. **C.R.K. Windows-Yule:** Writing – review & editing, Resources, Project administration, Methodology, Funding acquisition, Conceptualization. **M.J.H. Simmons:** Writing – review & editing, Resources, Project administration, Methodology, Funding acquisition, Supervision, Conceptualization.

Declaration of competing interest

The authors declare that they have no known financial interests or personal relationships that could influence the work reported in this paper.

Acknowledgements

The authors would like to thank the University of Birmingham's Positron Imaging Centre for the radiolabelling of the PEPT tracer particles. WJP is funded by both a University PhD scholarship from the School of Chemical Engineering at the University of Birmingham and IFP Energies Nouvelles. DK is funded by EPSRC Formulation Engineering Centre for Doctoral Training (Grant EP/S023070/1).

Computational resources for the PEPT data processing were provided by the University of Birmingham's Birmingham Environment for Academic Research (BEAR) service. BEAR provides flexible computational resources for the University of Birmingham research community. Additional information can be provided here: http://www.birmingham.ac.uk/bear.

Appendix A. Supplementary data

Supplementary data to this article can be found online at https://doi.org/10.1016/j.ces.2026.123846.

Data availability

Data will be made available on request.

References

Adams, L.W., Barigou, M., 2007. CFD analysis of caverns and pseudo-caverns developed during mixing of non-Newtonian fluids. Chem. Eng. Res. Des. 85 (5), 598–604. https://doi.org/10.1205/cherd06170.

Alauddin, M.M., 2012. Positron emission tomography (PET) imaging with ^{18}F-based radiotracers. Am. J. Nucl. Med. Mol. Imaging 2 (1), 55–76.

Alves, S.S., Maia, C.I., Vasconcelos, J.M.T., Serralheiro, A.J., 2002. Bubble size in aerated stirred tanks. Chem. Eng. J. 89 (1–3), 109–117. https://doi.org/10.1016/S1385-8947(02)00008-6.

Amanullah, A., Hjorth, S.A., Nienow, A.W., 1998. A new mathematical model to predict cavern diameters in highly shear thinning, power law liquids using axial flow impellers. Chem. Eng. Sci. 53 (3), 455–469. https://doi.org/10.1016/S0009-2509(97)00200-5.

Arlov, D., Revstedt, J., Fuchs, L., 2008. Numerical simulation of a gas-liquid Rushton stirred reactor – LES and LPT. Comput. Fluids 37 (7), 793–801. https://doi.org/10.1016/j.compfluid.2007.03.017.

Ascanio, G., 2015. Mixing time in stirred vessels: a review of experimental techniques. Chin. J. Chem. Eng. 23, 1065–1076. https://doi.org/10.1016/j.cjche.2014.10.022.

Aubin, J., Mavros, P., Fletcher, D.F., Bertrand, J., Xuereb, C., 2001. Effect of axial agitator configuration (up-pumping, down-pumping, reverse rotation) on flow patterns generated in stirred vessels. Chem. Eng. Res. Des. 79 (8), 845–856. https://doi.org/10.1205/02638760152721046.

Aubin, J., Xuereb, C., 2006. Design of multiple impeller stirred tanks for the mixing of highly viscous fluids using CFD. Chem. Eng. Sci. 61 (9), 2913–2920. https://doi.org/10.1016/j.ces.2005.10.075.

Aubin, J., Le Sauze, N., Bertrand, J., Fletcher, D.F., Xuereb, C., 2004. PIV measurements of flow in an aerated tank stirred by a down- and an up-pumping axial flow impeller. Exp. Therm Fluid Sci. 28 (5), 447–456. https://doi.org/10.1016/j.expthermflusci.2001.12.001.

Bashiri, H., Alizadeh, E., Bertrand, F., Chaouki, J., 2016. Investigation of turbulent fluid flows in stirred tanks using a non-intrusive particle tracking technique. Chem. Eng. Sci. 140, 233–251. https://doi.org/10.1016/j.ces.2015.10.005.

Bisgaard, J., Muldbak, M., Tajsoleiman, T., Rydal, T., Rasmussen, T., Huusom, J.K., Gernaey, K.V., 2021. Characterization of mixing performance in bioreactors using flow-following sensor devices. Chem. Eng. Res. Des. 174, 471–485. https://doi.org/10.1016/j.cherd.2021.08.008.

Bremer, J., Turek, T., 2024. From bodenstein to péclet – dimensionless numbers for axial dispersion in chemical reactors. Chem. Ing. Tech. 96 (12), 1562–1569. https://doi.org/10.1002/cite.202400102.

Buffo, M.M., Correa, L.J., Esperança, M.N., Cruz, A.J.G., Farinas, C.S., Badino, A.C., 2016. Influence of dual-impeller type and configuration on oxygen transfer, power consumption and shear rate in a stirred tank bioreactor. Biochem. Eng. J. 114, 130–139. https://doi.org/10.1016/j.bej.2016.07.003.

Bujalski, W., Konno, M., Nienow, A.W., 1988. Scale-up of 45° pitch blade agitators for gas dispersion and solid suspension. In: Proceedings of the 6Th European Conference on Mixing, pp. 389–398.
Cabaret, F., Bonnot, S., Fradette, L., Tanguy, P.A., 2007. Mixing time analysis using colorimetric methods and image processing. Ind. Eng. Chem. Res. 46 (14), 5032–5042. https://doi.org/10.1021/ie0613265.
Campesi, A., Cerri, M.O., Hokka, C.O., Badino, A.C., 2009. Determination of the average shear rate in a stirred and aerated tank bioreactor. Bioprocess Biosyst. Eng. 32, 241–248. https://doi.org/10.1007/s00449-008-0242-4.
Cancela, M.A., Alvarez, E., Maceiras, R., 2005. Effect of temperature and concentration on carboxymethylcellulose with sucrose rheology. J. Food Eng. 71, 419–424. https://doi.org/10.1016/j.jfoodeng.2004.10.043.
Cappello, V., Plais, C., Vial, C., Augier, F., 2021. Scale-up of aerated bioreactors: CFD validation and application to the enzyme production by Trichoderma reesei. Chem. Eng. Sci. 229, 116033. https://doi.org/10.1016/j.ces.2020.116033.
Charalambidou, A.-D., Wyrobnik, T.A., Micheletti, M., Ducci, A., 2024. Investigation of the impact of probes and internals on power and flow in stirred tank reactors. Chem. Eng. Sci. 286, 119683. https://doi.org/10.1016/j.ces.2023.119683.
Chiti, F., Bakalis, S., Bujalski, W., Barigou, M., Eaglesham, A., Nienow, A.W., 2011. Using positron emission particle tracking (PEPT) to study the turbulent flow in a baffled vessel agitated by a Rushton turbine: improving data treatment and validation. Chem. Eng. Res. Des. 89, 1947–1960. https://doi.org/10.1016/j.cherd.2011.01.015.
Chiti, F., Bakalis, S., Bujalski, W., Barigou, M., Eaglesham, A., Nienow, A.W., 2011. Using positron emission particle tracking (PEPT) to study the turbulent flow in a baffled vessel agitated by a Rushton turbine: improving data treatment and validation. Chem. Eng. Res. Des. 89 (10), 1947–1960. https://doi.org/10.1016/j.cherd.2011.01.015.
Chung, K.H.K., Simmons, M.J.H., Barigou, M., 2009. Local gas and liquid phase velocity measurement in a miniature stirred vessel using PIV combined with a new image processing algorithm. Exp. Therm Fluid Sci. 33 (2009), 743–753. https://doi.org/10.1016/j.expthermflusci.2009.01.010.
Cole, K., Brito-Parade, P.R., Hadler, K., Mesa, D., Neethling, S.J., Norori-McCormac, A. M., Cillers, J.J., 2022. Characterisation of solid hydrodynamics in a three-phase stirred tank reactor with positron emission particle tracking (PEPT). Chem. Eng. J. 433, 133819. https://doi.org/10.1016/j.cej.2021.133819.
Colombet, D., Legendre, D., Risso, F., Cockx, A., Guiraud, P., 2015. Dynamic and mass transfer of rising bubbles in a homogeneous swarm at large gas volume fraction. J. Fluid Mech. 763, 254–285.
Cooke, M., 1988. Mixing and mass transfer in filamentous fermentation. 2nd International Conference on Bioreactor Fluid Dynamics. pp. 37–64.
Coroneo, M., Montante, G., Paglianti, A., Magelli, F., 2011. CFD prediction of fluid flow and mixing in stirred tanks: numerical issues about the RANS simulations. Comput. Chem. Eng. 35, 1959–1968. https://doi.org/10.1016/j.compchemeng.2010.12.007.
Delaplace, G., Jeantet, R., Grenville, R., Cuvelier, G., Loubiere, K., 2020. How dimensional analysis allows to go beyond Metzner-Otto concept for non-Newtonian fluids. Rev. Chem. Eng. 38, 407–429. https://doi.org/10.1515/revce-2020-0006.
Delbridge, J.N., Barrett, T.A., Ducci, A., Micheletti, M., 2023. Power, mixing and flow dynamics of the novel Allegro stirred tank reactor. Chem. Eng. Sci. 271, 118545. https://doi.org/10.1016/j.ces.2023.118545.
Fangary, Y.S., Barigou, M., Seville, J.P.K., Parker, D.J., 2000. Fluid trajectories in a stirred vessel of non-Newtonian liquid using positron emission particle tracking. Chem. Eng. Sci. 55, 5969–5979. https://doi.org/10.1016/S0009-2509(00)00176-7.
Fishwick, R.P., Winterbottom, J.M., Stitt, E.H., 2003. Effect of gassing rate on solid-liquid mass transfer coefficients and particle slip velocities in stirred tank reactors. Chem. Eng. Sci. 58 (3–6), 1087–1093. https://doi.org/10.1016/S0009-2509(02)00651-6.
Fishwick, R.P., Winterbottom, J.M., Parker, D.J., Fan, X., Stitt, E.H., 2005. Hydrodynamic measurements of up- and down-pumping pitched-blade turbines in gassed, agitated vessels, using positron emission particle tracking. Ind. Eng. Chem. Res. 44 (16), 6371–6380. https://doi.org/10.1021/ie049191v.
Fitschen, J., Hofmann, S., Wutz, J., Kameke, A.V., Hoffmann, M., Wucherpfennig, T., Schluter, M., 2021. Novel evaluation method to determine the local mixing time distribution in stirred tank reactors. Chem. Eng. Sci.: X 10, 100098. https://doi.org/10.1016/j.cesx.2021.100098.
Gabelle, J.-C., Augier, F., Carvalho, A., Rousset, R., Morchain, J., 2011. Effect of tank size on k_La and mixing time in aerated stirred reactors with non-Newtonian fluids. Can. J. Chem. Eng. 89 (5), 1139–1153. https://doi.org/10.1002/cjce.20571.
Gabelle, J.-C., Jourdier, E., Licht, R.B., Ben Chaabane, F., Henaut, I., Morchain, J., Augier, F., 2012. Impact of rheology on the mass transfer coefficient during the growth phase of Trichoderma reesei in stirred bioreactors. Chem. Eng. Sci. 75, 408–417. https://doi.org/10.1016/j.ces.2012.03.053.
Godleski, E.S., Smith, J.C., 1962. Power requirements and blend times in the agitation of pseudoplastic fluids. AIChE J. 8 (5), 617–620. https://doi.org/10.1002/aic.690080511.
Grenville, R., 1992. Blending of viscous Newtonian and pseudo-plastic fluids. Cranfield University. PhD Thesis.
Guha, D., Ramachandran, P.A., Dudukovic, M.P., 2007. Flow field of suspended solids in a stirred tank reactor by Lagrangian tracking. Chem. Eng. Sci. 62 (22), 6143–6154. https://doi.org/10.1016/j.ces.2007.06.033.
Guida, A., Fan, X., Parker, D.J., Nienow, A.W., Barigou, M., 2009. Positron emission particle tracking in a mechanically agitated solid-liquid suspension of coarse particles. Chem. Eng. Res. Des. 87 (4), 421–429. https://doi.org/10.1016/j.cherd.2008.12.001.
Guida, A., Nienow, A.W., Barigou, M., 2010. PEPT measurements of solid-liquid flow field and spatial phase distribution in concentrated monodisperse stirred suspensions. Chem. Eng. Sci. 65 (6), 1095–1914. https://doi.org/10.1016/j.ces.2009.11.005.
Hardy, N., Augier, F., Nienow, A.W., Beal, C., Ben Chaabane, F., 2017. Scale-up agitation criteria for Trichoderma reesei fermentation. Chem. Eng. Sci. 172, 158–168. https://doi.org/10.1016/j.ces.2017.06.034.
Haringa, C., Tang, W., Deshmukh, A.T., Xia, J., Reuss, M., Heijnen, J.J., Mudde, R.F., Noorman, H.J., 2016. Euler-Lagrange computational fluid dynamics for (bio)reactor scale down: an analysis of organism lifelines. Eng. Life Sci. 16, 652–663. https://doi.org/10.1002/elsc.201600061.
Hartmann, H., Derksen, J.J., van den Akker, H.E.A., 2006. Mixing times in a turbulent stirred tank by means of LES. AIChE J 52 (11), 3696–3706. https://doi.org/10.1002/aic.10997.
Hart-Villamil, R., Ingram, A., Windows-Yule, C., Gupta, S., Nicusan, A.L., 2024. On the autonomous validation and comparison of particle models for a Newtonian laminar flow mixing model using PEPT. Chem. Eng. Res. Des. 206, 139–150. https://doi.org/10.1016/j.cherd.2024.04.023.
Hofmann, S., Rautenbach, R., Buntkiel, L., Brouwers, I.S., Gaugler, L., Barczyk, J., Fitschen, J., Reinecke, S., Hoffmann, M., Takors, R., Hampel, U., Schluter, M., 2025. Lagrangian sensor particles for detecting hydrodynamic heterogeneities in industrial bioreactors: experimental analysis and Lattice-Boltzmann simulations. Chem. Eng. J. Adv. 22, 100744. https://doi.org/10.1016/j.ceja.2025.100744.
Jadhav, A.J., Barigou, M., 2022. Eulerian-Lagrangian modelling of turbulent two-phase particle-liquid flow in a stirred vessel: CFD and experiments compared. Int. J. Multiph. Flow 155, 104191. https://doi.org/10.1016/j.ijmultiphaseflow.2022.104191.
Jamshed, A., Cooke, M., Ren, Z., Rodgers, T.L., 2018. Gas-liquid mixing in dual agitated vessels in the heterogeneous regime. Chem. Eng. Res. Des. 133, 55–69. https://doi.org/10.1016/S1385-8947(02)00008-6.
Khopkar, A., Rammohan, A., Ranade, V., Dudukovic, M., 2005. Gas-liquid flow generated by a Rushton turbine in stirred vessel: CARPT/CT measurements and CFD simulations. Chem. Eng. Sci. 60, 2215–2229. https://doi.org/10.1016/j.ces.2004.11.044.
Kukukova, A., Noël, B., Kresta, S.M., Aubin, J., 2008. Impact of sampling method and scale on the measurement of mixing and the coefficient of variance. AIChE J 54 (12), 3068–3083. https://doi.org/10.1002/aic.11639.
Kukukova, A., Aubin, J., Kresta, S.M., 2009. A new definition of mixing and segregation: three dimensions of a key process variable. Chem. Eng. Res. Des. 87, 633–647. https://doi.org/10.1016/j.cherd.2009.01.001.
Kuschel, M., Fitschen, J., Hoffmann, M., von Kameke, A., Schluter, M., Wucherpfennig, T., 2021. Validation of novel lattice boltzmann large eddy simulations (LB LES) for Equipment characterization in biopharma. Processes 9 (6), 950. https://doi.org/10.3390/pr9060950.
Lee, K.C., Yianneskis, M., 1997. A liquid crystal thermographic technique for the measurement of mixing characteristics in stirred vessels. Chem. Eng. Res. Des. 75 (8), 746–754. https://doi.org/10.1205/026387697524416.
Liu, L., Barigou, M., 2013. Numerical modelling of velocity field and phase distribution in dense monodisperse solid-liquid suspensions under different regimes of agitation: CFD and PEPT experiments. Chem. Eng. Sci. 101, 837–850. https://doi.org/10.1016/j.ces.2013.05.066.
Losoi, P., Konttinen, J., Santala, V., 2024. Modeling large-scale bioreactors with diffusion equations. Part I: predicting axial dispersion coefficient and mixing times. Biotechnol. Bioeng. 121 (3), 1060–1075. https://doi.org/10.1002/bit.28632.
Magelli, F., Montante, G., Pinelli, D., Paglianti, A., 2013. Mixing time in high aspect ratio vessels stirred with multiple impellers. Chem. Eng. Sci. 101, 712–720. https://doi.org/10.1016/j.ces.2013.07.022.
Martin, T.W., Seville, J.P.K., Parker, D.J., 2007. A general method for quantifying dispersion in multiscale systems using trajectory analysis. Chem. Eng. Sci. 62 (13), 3419–3428. https://doi.org/10.1016/j.ces.2007.02.050.
Metzner, A., Otto, R., 1957. Agitation of non-newtonian fluids. AIChE J. 3, 3–10. https://doi.org/10.1002/aic.690030103.
Moilanen, P., Laakkonen, M., Aittamaa, J., 2006. Modeling aerated fermenters with computational fluid dynamics. Ind. Eng. Chem. Res. 45 (25), 8656–8663. https://doi.org/10.1021/ie060097j.
Montante, G., Paglianti, A., 2015. Gas hold-up distribution and mixing time in gas-liquid stirred tanks. Chem. Eng. J. 279, 648–658. https://doi.org/10.1016/j.cej.2015.05.058.
Nere, N., Patwardhan, A., Joshi, J., 2003. Liquid-phase mixing in stirred vessels: turbulent flow regime. Ind. Eng. Chem. Res. 42, 2661–2698. https://doi.org/10.1021/ie0206397.
Nicuşan, A.L., Windows-Yule, C.R.K., 2020. Positron emission particle tracking using machine learning. Rev. Sci. Instrum. 91 (1), 013329. https://doi.org/10.1063/1.5129251.
Nienow, A.W., 1997. On impeller circulation and mixing effectiveness in the turbulent flow regime. Chem. Eng. Sci. 52 (15), 2557–2565. https://doi.org/10.1016/S0009-2509(97)00072-9.
Nienow, A.W., Warmoeskerken, M.M.C.G., Smith, J.M., Konno, M., 1985. On the flooding/loading transition and the complete dispersal condition in aerated vessels agitated by a Rushton turbine. Proceedings of 5th European Mixing Conference, Germany. pp. 143–154. BHRA, ISBN: 9780947711047.
Parker, D.J., Broadbent, C., Fowles, P., Hawkesworth, M., McNeil, P., 1993. Positron emission particle tracking – a technique for studying flow within engineering equipment. Nucl. Instrum. Methods Phys. Res. Sect. 326 (3), 592–607. https://doi.org/10.1016/0168-9002(93)90864-E.
Parker, D., Forster, R., Fowles, P., Takhar, P., 2002. Positron emission particle tracking using the new Birmingham positron camera. Nucl. Inst. Methods Phys. Res. A 477, 540–545. https://doi.org/10.1016/S0168-9002(01)01919-2.
Patwardhan, A.W., 2001. Prediction of residence time distribution of stirred reactors. Ind. Eng. Chem. Res. 40, 5686–5695. https://doi.org/10.1021/ie0103198.

Paul, E.L., Atiemo-Obeng, V.A., Kresta, S., 2004. Handbook of industrial mixing; science and practice. John Wiley & Sons.

Peace, W.J., Jones, R.O., Augier, F., Simmons, M.J.H., Windows-Yule, C.R.K., 2025. Study of the dispersed and flooded aeration regimes in two-phase gas-liquid stirred tanks using positron emission particle tracking. Chem. Eng. Res. Des. 219, 546–556. https://doi.org/10.1016/j.cherd.2025.06.037.

Poulsen, B.R., Iversen, J.J.L., 1997. Mixing determinations in reactor vessels using linear buffers. Chem. Eng. Sci. 52 (6), 979–984. https://doi.org/10.1016/S0009-2509(96)00466-6.

Rammohan, A., Kemoun, A., Al-Dahhan, M., Dudukovic, M., 2001. A Lagrangian description of flows in stirred tanks via computer-automated radioactive particle tracking (CARPT). Chem. Eng. Sci. 56, 2629–2639. https://doi.org/10.1016/S0009-2509(00)00537-6.

Ramsay, J., Simmons, M.J.H., Ingram, A., Stitt, E.H., 2016. Mixing of Newtonian and viscoelastic fluids using "butterfly" impellers. Chem. Eng. Sci. 139 (2016), 125–141. https://doi.org/10.1016/j.ces.2015.09.026.

Rosseburg, A., Fitschen, J., Wutz, J., Wucherpfennig, T., Schluter, M., 2018. Hydrodynamic inhomogeneities in large scale stirred tanks – influence on mixing time. Chem. Eng. Sci. 188, 208–220. https://doi.org/10.1016/j.ces.2018.05.008.

Roussinova, V., Kresta, S.M., 2008. Comparison of continuous blend time and residence time distribution models for a stirred tank. Ind. Eng. Chem. Res. 47, 3552. https://doi.org/10.1021/ie070955r.

Rushton, J.H., Costich, E.W., Everett, H.J., 1950. Power characteristics of mixing impellers; Part II. Chem. Eng. Progr. 46 (9), 467–476.

S. Ruszkowski (1994) A rational method for measuring blending performance comparison of different impeller types. Proceedings of 8th European Mixing Conference; Institution of Chemical Engineers Symposium Series (136) pp. 283 – 291, Rugby, UK.

Sánchez Pérez, J.A., Rodriguez Porcel, E.M., Casas Lopez, J.L., Fernandez Sevilla, J.M., Chisti, Y., 2006. Shear rate in stirred tank and bubble column bioreactors. Chem. Eng. J. 124 (1–3), 1–5. https://doi.org/10.1016/j.cej.2006.07.002.

Shewale, S.D., Pandit, A.B., 2006. Studies in multiple impeller agitated gas-liquid contactors. Chem. Eng. Sci. 61 (2), 489–504. https://doi.org/10.1016/j.ces.2005.04.078.

Simmons, M.J.H., Edwards, I., Hall, J.F., Fan, X., Parker, D.J., Stitt, E.H., 2009. Techniques for visualisation of cavern boundaries in opaque industrial mixing systems. AIChE J. 55 (11), 2765–2772. https://doi.org/10.1002/aic.11889.

Vasconcelos, J.M.T., Alves, S.S., Barata, J.M., 1995. Mixing in gas-liquid contactors agitated by multiple turbines. Chem. Eng. Sci. 50 (14), 2343–2354. https://doi.org/10.1016/0009-2509(95)00090-R.

Wadnerkar, D., Utikar, R.P., Tade, M.O., Pareek, V.K., 2012. CFD simulation of solid-liquid stirred tanks. Adv. Powder Technol. 23 (4), 445–453. https://doi.org/10.1016/j.apt.2012.03.007.

D. Werner, D. Weston (2022) Up4: Universal Post-Processor for Particulate Processes. URL: https://github.com/uob-positron-imaging-centre/up4.

Windows Yule, C.R.K., Herald, M.T., Nicuşan, A.L., Wiggins, C.S., Pratx, G., Manger, S., Odo, A.E., Leadbeater, T., Pellico, J., de Rosales, R.T.M., Renaud, A., Govender, I., Carasik, L.B., Ruggles, A.E., Kokalova-Wheldon, T.Z., Seville, J.P.K., Parker, D.J., 2021. Recent advances in positron emission particle tracking: a comparative review. Rep. Prog. Phys. https://doi.org/10.1088/1361-6633/ac3c4c.

Windows-Yule, C.R.K., Seville, J.P.K., Ingram, A., Parker, D.J., 2020. Positron emission particle tracking of granular flows. Annu. Rev. Chem. Biomol. Eng. 11, 367–396. https://doi.org/10.1146/annurev-chembioeng-011620-120633.

Yoon, H.S., Balachandar, S., Ha, M.Y., 2015. Large eddy simulation of passive scalar transport in a stirred tank for different diffusivities. Int. J. Heat Mass Transf. 91, 885–897. https://doi.org/10.1016/j.ijheatmasstransfer.2015.08.030.

Zak, A., Alberini, F., Maluta, F., Moucha, T., Montante, G., Paglianti, A., 2022. Liquid mixing time and gas distribution in aerated multiple-impeller stirred tanks. Chem. Eng. Res. Des. 184, 501–512. https://doi.org/10.1016/j.cherd.2022.06.021.

Zak, A., Valenz, L., Moucha, T., Zednikova, M., 2025. Gas phase behaviour in environment of fermentation processes. Chem. Eng. Res. Des. 219, 43–51. https://doi.org/10.1016/j.cherd.2025.05.031.

Zhang, A., Tsang, V.L., Korke-Kshirsagar, R., Ryll, T., 2014. Effects of pH probe lag on bioreactor mixing time estimation. Process Biochem. 49, 913–916. https://doi.org/10.1016/j.procbio.2014.03.005.

Zhang, Q., Yong, Y., Mao, Z.-S., Yang, C., Zhao, C., 2009. Experimental determination and numerical simulation of mixing time in a gas-liquid stirred tank. Chem. Eng. Sci. 64 (12), 2926–2933. https://doi.org/10.1016/j.ces.2009.03.030.

Zhao, D., Gao, Z., Muller-Steinhagen, H., Smith, J.M., 2001. Liquid-phase mixing times in sparged and boiling agitated reactors with high gas loading. Ind. Eng. Chem. Res. 40 (6), 1482–1487. https://doi.org/10.1021/ie000445w.